Korean J. Chem. Eng., 38(9), 1797-1809 (2021)
DOI: 10.1007/s11814-021-0842-0

pISSN: 0256-1115
eISSN: 1975-7220

Effect of temperature and feed rate on pyrolysis oil produced via helical screw fluidized bed reactor

Khan Muhammad Qureshi*, Andrew Ng Kay Lup,***,†, Saima Khan*, Faisal Abnisa****, and Wan Mohd Ashri Wan Daud*,†**

*Department of Chemical Engineering, Faculty of Engineering, University of Malaya, 50603, Kuala Lumpur, Malaysia
**School of Energy and Chemical Engineering, Xiamen University Malaysia, Jalan Sunsuria, Bandar Sunsuria, 43900 Sepang, Selangor Darul Ehsan, Malaysia
***College of Chemistry and Chemical Engineering, Xiamen University, Xiamen, 361005, Fujian, China
****Department of Chemical and Materials Engineering, Faculty of Engineering, King Abdulaziz University, Rabigh, 21911, Saudi Arabia
(*Received 5 March 2021 • Revised 9 May 2021 • Accepted 11 May 2021*)

Abstract−A series of experiments was conducted to study the effect of temperature and feed rate on physicochemical properties and yield of bio-oil. The experiments were performed in a helical screw fluidized bed reactor and about 150-gram palm shell (PS) was pyrolyzed in each run at 275 °C/min heating rate. The first set of experiments was conducted at temperature ranging from 400 to 650 °C without using any inert gas for fluidization. While the second set of experiments were performed at feed rates ranging from 3 to 25 g/min in order to investigate the effects of feed rate on pyrolytic products. Results showed that the bio-oil yield was increased with the increase in temperature and feed rate due to the enhanced biomass volatilization. In a similar vein to this, a greater extent in oxygenates cracking was also noted in the bio-oil. A maximum liquid yield of about 72.84 wt% was obtained at 500 °C, while 72.92 wt% liquid yield was obtained with 25 g/min feed rate. The HHV of bio-oil was also increased from 38.52 to 43.13 MJ/kg when pyrolysis temperature was increased from 400 to 650 °C.

Keywords: Pyrolysis, Temperature, Feed Rate, Helical Screw Fluidized Bed Reactor Pyrolytic Products

INTRODUCTION

Biomass waste can be considered as an attractive feedstock for the production of heat, energy, fuels or value-added products [1]. Thermochemical conversion of biomass is widely used due to several advantages, such as faster chemical processes, use of whole biomass to obtain different products and the possibility to use in a combination of biomass and renewables [2]. Among the several thermochemical processes, pyrolysis with the use of fluidized system is a promising method [3]. However, one of the main issues with the conventional fluidized bed process is its energy intensive nature due to gas fluidization and particulate cyclonic separation. For conventional fluidized bed reactors many studies have been conducted on operating parameters for upgrading of pyrolysis products from laboratory to industrial scale. In view of these challenges, helical screw fluidization technique was proposed as an innovative method in the previous work by the author. This method involves the use of mechanical power for fluidization of biomass sample within the reactor shell which is being isolated from the ingress of oxygen and no gas required for fluidization and extra devices for particulate separation [4].

Many studies have been dedicated to the effect of operating parameters, and every single parameter has its own significance in the pyrolysis process. Operating parameters are not only responsible for maximizing the liquid yield but also affecting pyrolysis efficiency and composition of product quality [5,6]. The relative amount of each product produced depends upon operating parameters, properties of biomass and type of pyrolysis process. The pyrolysis of biomass is influenced by a large number of factors and among all other things, temperature and feed rate have been shown to have significant impact on thermal conversion of biomass to bio-oil [7]. Temperature is one of the most significant operating parameters in pyrolysis since it controls the cracking reaction of the tar [8], and different types of biomass have different degradation temperatures depending on their composition and chemical structure. Jahirul et al. showed that the yield and the quality of pyrolysis oil clearly vary with temperature. Therefore, more research is required to obtain a complete description of thermochemical conversion processes to yield high quality bio-oil [9].

The optimum temperature range for pyrolysis is 500-550 °C, which gives maximum liquid yield. An increase in feed temperature will shift to gasification process, which reduces the liquid yield since cellulose and hemicellulose both are responsible to produce more volatiles at low temperature as compared to lignin [10]. Usually, decomposition of biomass at medium temperature (400-550 °C) favors the production of bio-oils at short residence times. Montoya et al. also suggested the average temperatures among 500-550 °C typically increase the bio-oil yield [11]. At higher temperature, the

†To whom correspondence should be addressed.
E-mail: andrew.ng@xmu.edu.my, ashri@um.edu.my

probability of gas production increases [12]. However, at low temperature, by-product biochar formation is significant [13]. To change the pyrolytic composition, the optimization of reaction temperature and feed rate is essential [14].

Bridgewater indicated that woody biomass is mostly transformed into liquid product (<70 wt% yield) at 500 °C on dry feed basis [15]. Typically, at low temperature of <300 °C, fragmentation of biomass at heteroatom sites occurs inside the biomass structure, which leads to heavy tar formation. Above 455 °C, sufficient disintegration of biomass subsequently results in high molecular disruption, leading to various types of useful compounds in the liquid yield. At such high temperature, pyrolysis reactions transform the product composition. This modification of pyrolysis temperature possibly will decrease the by-product biochar formation and support the formation of liquid product [16]. Bhattachrjee et al. studied the influence of temperature on red seaweed residues by means of a thermogravimetric analyzer with fast pyrolysis in the temperature range of 450-650 °C in helium atmosphere. They found that the product yield distribution is a function of the biomass feedstock and the liquid yield is about 70 wt% when temperature reaches 550 °C [17].

Muasengerere et al. performed pyrolysis of corn stover and the maximum bio-oil yield was obtained at 550 °C. The decrease in the bio-oil yield at high temperature was due to the secondary thermal cracking reactions of condensable gases and tar fragments which formed more vapors and increased the non-condensable gas yield [18]. Heidari et al. studied the influence of temperature on fast pyrolysis of Eucalyptus wood in a continuous fluidized bed reactor and observed a decline in liquid yield with the increase of temperature from 450 to 600 °C, while gas yield was noticeably improved from 29.4 to 48.4 wt%. The increase in gas yield was due to the secondary cracking of pyrolysis vapors. Furthermore, an increase in temperature was accompanied by a reduction in the amount of by-product biochar yield from 19.7 to 14.2 wt% [6,19]. Zhou et al. also informed that the increase in non-condensable gas is linked to increased pyrolysis temperature irrespective of the heating method used [20].

Feed rate is a parameter that is less studied though it can affect the pyrolysis reactions and product formation. Furthermore, feed rate can affect the fluidization behavior, which affects heat and mass transfer rate, vapor residence time and secondary reaction. Better heat distribution is made possible at lower biomass feed rate, which results in quicker de-volatilization, leading to the formation of gas and organic vapors. In addition, the low feed rate may decrease the movement of pyrolytic vapor and boost the secondary reaction, which decreases the bio-oil yield [6]. However, the formation of bio-oil and gas product with high feed rate is higher than that of low feed rate. This is due to the higher volatile residence time at low feed rate condition. It shows that the volatile-by-product biochar interaction is considerably lengthier and that leads to the repolymerization of volatiles, thus resulting in an increased quantity of by-product biochar. The increase in biomass feed rate enables higher condensable vapor formation and shorter vapor residence time inside the reactor, thus minimizing secondary cracking reactions, which leads to higher bio-oil yield [21].

Therefore, systematic study is required to optimize the feed rate in a continuous pyrolysis process. Qingang et al. investigated the effect of different feed rates ranging from 1.6 to 2.7 kg/h on pyrolysis yields using 42% cellulose, 34% hemicellulose and 24% lignin with 0.5 mm particle size at 500 °C in bubbling fluidized bed reactor. They noticed that biomass feed rate has negligible effect on pyrolytic products when it is less than 1.92 kg/h. This may be because adequate heat transfers from the reactor wall to biomass, which increases the decomposition. However, when feeding rate is more than 1.92 kg/h, an adverse effect of biomass feed rate on formation of tar and by-product biochar yield was noticed. At high feeding rate, there was higher degree of spatial disorder of feed in the bed temperature, which may result in poorer heat transfer to biomass. Therefore, biomass feed rate needs to be tuned at an even-handed level for a suitable product yield [22]. Aghdas et al. also performed fast pyrolysis of Eucalyptus wood in fluidized reactor at temperature of 450 °C and attained higher liquid yield of 70 wt% at 90 g/min feed rate. However, a further increase in feed rate to 100 g/h showed a substantial decline in liquid yield and an increase in by-product biochar yield from 15 wt% to 20 wt% [19]. These findings showed that the feed rate is a significant parameter in obtaining higher bio-oil yield.

The use of a novel helical screw-fluidized bed reactor (HSFBR) was proposed for slow pyrolysis mode and its design was studied in our previous work [23]. Apart from the capability to get high liquid yield, the novelty of the helical screw fluidized bed reactor is fast vapor production, low pyrolysis time, non-particle agglomeration, non-occurrence of pressure drop during process execution and low byproduct char formation. In addition, the novelty of this reactor can also be clearly observed from the obtained quality of liquid product that confined high organic phase, low water content, and high energy density. Most of the pyrolysis researches were conducted in a fixed bed or gas fluidized bed systems. This study's aim was to investigate the effect of operating parameters: temperature and feeding rate on the physicochemical properties and the yield of bio-oil. Furthermore, this study also emphasized the selected operating parameters to learn how to produce pyrolytic liquid product of higher homogeneity, quality, quantity and desired characteristics using novel helical screw fluidized bed reactor (HSFBR) in semi-continuous pyrolysis mode.

MATERIAL AND METHODS

1. Raw Material Collection and Analysis

The palm shell (PS) waste was obtained from Felcra Palm Oil Mill Sdn. Bhd., Bota, Perak, Malaysia. The samples were washed and dehydrated under sun for four days to decrease the moisture content. Dried samples were subsequently ground and sieved using U.K standard sieve to get the 1-2 mm range particle size and dried again in an oven at 110 °C for 4 h to further reduce the remaining moisture content below to 10%.

2. Pyrolysis Experiment

The experimental setup of this study and the design features of novel helical screw fluidized bed reactor (HSFBR) are illustrated in Fig. 1 along with the main operating temperatures monitored during the pyrolysis process. The reactor is made from stainless steel (CS309) of 5 mm thickness with an internal diameter of 228 mm

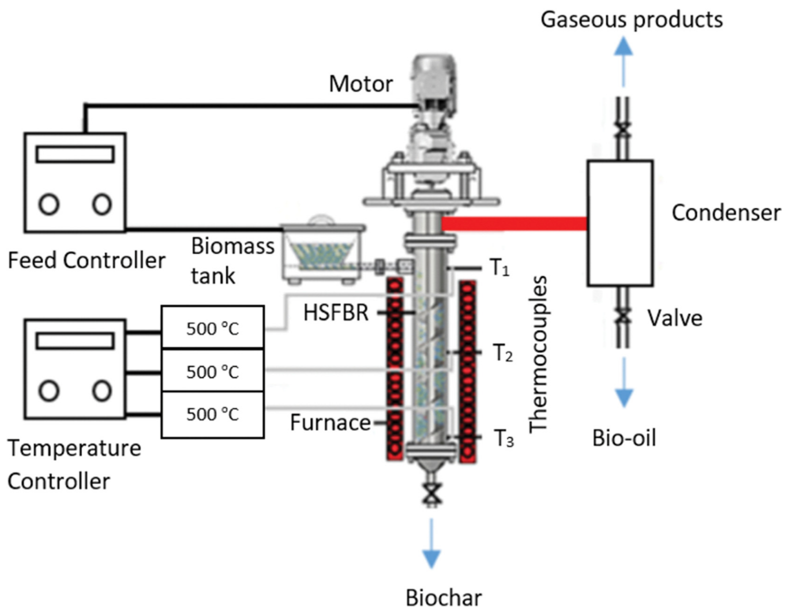

Fig. 1. Schematic diagram of novel helical fluidized bed pyrolysis reactor.

and total length of 1,524 mm. A helical screw of stainless steel (CS309) with total length of 1,550 mm containing six flights with equal pitch distance of 95.25 mm and an external diameter of 203.2 mm was used. A screen plate of 132.4 mm diameter with 1.5 mm pore size was placed inside the reactor bottommost end between the reactor and the by-product char collector to arrest or hold the material for a short period of time until biomass particles were reduced to 1-2 mm and to pass through the screen pores to the by-product biochar collector. For continuous biomass feed an auger feeding system was provided at the top to control biomass feed rate. The helical screw was powered by an AC motor. A pressure gauge of 7 bar/100 psi was installed between the reactor and condenser line to constantly monitor the vapor pressure. A series of two stainless steel condensers were installed and each condenser with a length of 1,371.6 mm and outside diameter of 228.6 mm. A chiller was provided to deliver chilled water at 5 °C temperature as cooling medium for rapid pyro vapor condensation to avoid secondary vapor cracking.

Each experiment was performed by loading 300 g of PS with an average particle size of 1-2 mm into the HSFBR. The reactor was heated with dual zone electric furnace of 1.5 KW power rating, and three K-type thermocouples were attached along the exterior of the reactor shell; temperature was monitored by a digital display. PID temperature controller (KT-1130, Korea CHINO Co.) was used to maintain a heating rate of 275 °C/min and to observe the isothermal reaction conditions. Furthermore, in the first set of experiments, different temperatures were used from 400, 450, 500, 550, 600 and 650 °C in order to optimize the temperature without using any inert gas for fluidization at 150 g PS biomass loading and feed rate of 25 g/min. In the second set of experiments the temperature was fixed at 500 °C with different feed rates at 3, 5, 7, 10, 13, 15, 18, 20, 23 and 25 g/min. Temperature range of 400-650 °C and feed rate of 3-25 g/min were chosen as the typical operating condition ranges for effective biomass pyrolysis [6,23].

After the set condition was reached, the experiment was continued for another 10 minutes to condense all condensates. The vapor was collected in the condensers while non-condensable gases were left with controlled flow rate of 20 cc/min, and gas samples were collected in a sample bag for offline gas analysis. The by-product biochar was collected simultaneously through the by-product biochar collector as fitted at bottom of the reactor. The product yield of bio-oil and by-product biochar was calculated using Eq. (1), as follows:

$$Y_p = \frac{X_1}{X_2} \times 100 \tag{1}$$

where, Y_p is the product yield, X_1 is the mass of the chosen product, and X_2 is the initial weight of the raw material. The gas yield was calculated by subtraction: gas yield=100−(liquid yield+by-product biochar yield). The collected bio-oil and by-product biochar were tested for physicochemical analysis. Each pyrolysis experiment was repeated three times under the same operating condition.

3. Phase Separation and Physicochemical Characterization

The bio-oil received from the condensation unit was transferred into a separating funnel and allowed to settle for three days at ambient temperature to separate organic and aqueous phases under the action of gravity. After the phase separation of bio-oil, organic phase was characterized for physicochemical parameters such as density, viscosity, pH and water content. A density test was performed using a pycnometer of (25 mL) volume at room temperature based on the ASTM D4052 standard. The viscosity was determined according to ASTM D445 standard with rotational viscometer (model DV-II+Pro EXTRA) with 20 rpm at 26 °C temperature. The pH/acidity test was determined by using Metrohm 827 pH meter following ASTM E70 standard. The Karl Fischer titration method was used to measure the water content in bio-oil organic samples. This measurement was performed by 737 Karl fisher coulometer according to ASTM E203 (2001) standard [22,23].

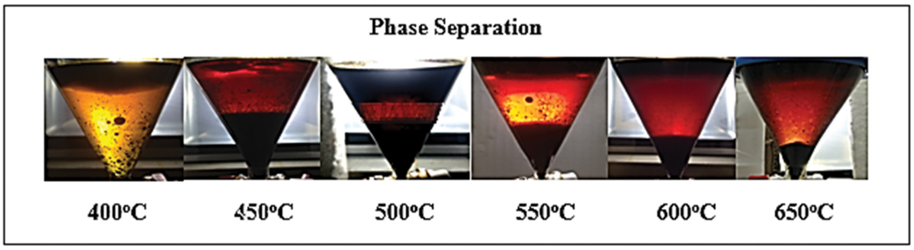

Fig. 2. Phase separation of bio-oil with various temperatures under the influence of gravity.

Chemical characterization of bio-oil and by-product biochar was performed by CHNOS elemental analysis, Fourier transform infrared (FTIR) spectroscopy, while GC-MS analysis was only used for bio-oil. Ultimate analysis was performed using Perkin-Elmer 2400 CHNS/O to obtain carbon, hydrogen, oxygen, nitrogen and sulfur data. Perkin-Elmer Spectrum 400 spectrometer was used for FTIR analysis and the samples were scanned in the range of 400-4,000 cm^{-1} with a resolution of 4 cm^{-1}. GC/MS was performed with Shimadzu model no. QP2010 equipped with DB-5 MS column (30 m× 0.25 mm×0.25 μm). The injector temperature of GC/MS was set at 250 °C and oven temperature was programmed at 60 °C for 1 minute and then increased to 300 °C with a heating rate of 10 °C/min and continued for 20 minutes. Helium was used as a carrier gas with a flow rate of 1.5 mL/min. The detector temperature was set at 230 °C. The sample was injected into the column with a split ratio of 1 : 30. The chemical composition of bio-oil was identified by comparing the sample chromatogram with the database in the GC/MS library.

To determine the fuel properties, bio-oil sample was subjected to several characterizations, which included fire point, flash point, dew point, pour point, higher heating value (HHV) and lower heating value (LHV). Flash point test was performed according to ASTM D93-97 standard using HFP 360 Pensky-Martens closed cup manual tester. Fire point test was performed based on ASTM D93 standard using Pensky Marten open cup tester. Dew point test was made in a batch glass distillation unit at atmospheric pressure following ASTM D02 standard for liquids. Pour point of bio-oil was determined according to ASTM-D97-17b method. HHV of bio-oil and by-product biochar using ultimate analysis was determined according to Dulong formula as shown in Eq. (2), while LHV was calculated by Eq. (3) proposed by Abnisa et al. [24].

$$\text{HHV (MJ/kg)} = \frac{338.2\times\text{C}+1{,}442.8\times\left(\text{H}-\frac{\text{O}}{8}\right)}{1{,}000} \tag{2}$$

$$\text{LHV (MJ/kg)} = \text{HHV} - 0.218\times\text{H} \tag{3}$$

TGA/DTG analysis was performed using TGA Q500 to investigate the by-product biochar for proximate analysis and thermal properties of the samples. Around 40 mg of each sample was used for this analysis and heated in an alumina crucible under N_2 atmosphere from 30 to 800 °C with a heating rate of 20 °C/min. Moisture content was estimated from the initial weight loss at 150 °C. Volatile matter was determined by the calculation of the weight loss data between 150 to 450 °C. Ash content was determined from available residue over combustion temperature of 800 °C [22]. The percentage of fixed carbon was calculated by Eq. (4).

$$\text{Fixed carbon (\%)} = 100 - (\text{Moisture content} + \text{Volatile matter} + \text{Ash}) \tag{4}$$

Analysis of non-condensable gas specifically hydrogen and methane was done using a gas analyzer, Rosemount Analytical X-STREAMTM (UK) apparatus.

RESULTS AND DISCUSSION

1. Phase Separation

Bio-oil derived at different temperatures showed differences in color as shown in Fig. 2. The bio-oil initially appeared as a single-phase dark brown, viscous free flowing liquid with strong bitter smell. The presence of water in the bio-oil is due to existing moisture in the biomass and dehydration and degradation of lignin during pyrolysis [4]. Phase separation showed that, the liquid was divided into two layers and then three layers based on the pyrolytic temperature. The black color represents the organic or hydrocarbon phase, while yellowish red layer represents the aqueous phase. These multilayers are due to the density variation and the presence of oxygenated compounds, which is attributed to pyrolytic temperature difference; therefore, bio oils have a polar affinity and form distinct phases [25]. Lu et al. also reported that multi layers were due to the variance in solubility or polar affinity among the different phases [26].

2. Product Yields

2-1. Effect of Temperature

Table 1 shows the product distribution at various temperatures. At 400 °C, the bio-oil yield was relatively low with a value of 39.1 wt%, while by-product biochar value was higher with 50 wt%. The higher value of by-product biochar can be attributed to the less

Table 1. Influence of temperature on bio-oil yield

Temperature (°C)	Product distribution (wt%)				
	Organic	Aqueous	Bio-oil*	Biochar	Gas
400	16.00	23.10	39.10	50.00	10.90
450	23.50	30.20	53.70	34.80	11.50
500	42.21	30.63	72.84	11.98	15.18
550	41.00	27.34	68.34	10.60	21.06
600	37.20	28.31	65.51	12.60	21.89
650	31.60	33.80	65.40	11.60	23.00

*Bio-oil=organic+aqueous

decomposition of cellulose between 300-450 °C [27]. As the temperature increased to 450 °C, bio-oil yield increased to 53.7 wt% while by-product biochar yield decreased from 50 to 34.8 wt%. This could be attributed to the breaking of glycoside chain of polysaccharide which provides tar production. Similar effects of temperature at 450 °C on product distribution are reported elsewhere [14]. Bio-oil yield drastically increased to 72.84 wt% when temperature reached 500 °C, and this could be attributed to the lignin decomposition between 250-500 °C, which is the major contributor of liquid at the end of pyrolysis [28,29]. Conversely the by-product biochar yield was drastically reduced to 22.82 wt%, while gas yield was slightly increased by approximately 3.68 wt%. Similar trend was also reported by Bridgewater et al. [30] and Powar et al. [31].

However, a further increase in temperature to 550 °C resulted in bio-oil yield to slightly reduce by 1.38 wt%, while the gas product yield increased to 5.88 wt%. This variation in liquid and gas yields can be explained by the onset of secondary cracking of vapors at 550 °C, which resulted in decline of the liquid product yield and increase in the non-condensable gas yield [32]. Similar trend was observed as temperature further increased to 650 °C and was also reported by Powar et al. [31].

According to Bridgwater et al., pyrolysis at adequate temperature of around 500 °C with short vapor residence time of up to 2 s is desirable to avoid the secondary reactions in vapor phase in order to produce high liquid products [30,33]. In addition, the effect of secondary reaction in vapor phase on bio-oil composition requires further investigation [34].

2-2. Effect of Feed Rate

The results of this study show that when feed rate was approximately about 3 g/min the bio-oil, by-product biochar and gas yields were 70.73, 23.32 and 5.95 wt% respectively as shown in Table 2. However, when the feed rate was in the range of 3-13 g/min it was observed that the liquid, by-product biochar and gas yields were relatively constant. This may be attributed to high heat transfer rate at low feed rate, which resulted in faster de-volatilization, leading to the formation of gas and vapors. In addition, at low feed rate it may decrease the movement of pyrolytic vapor and boost the secondary reaction, which decreases the bio-oil yield [6].

Table 2. Effect of feed rates on pyrolytic yield

	Product distribution (wt%)				
Feed rate (g/min)	Organics	Aqueous	Total Bio-oil	Biochar	Gas
3	44.56	26.17	70.73	23.32	5.95
5	45.26	23.13	68.39	27.56	4.05
7	45.06	23.24	68.30	26.32	5.38
10	45.11	23.73	68.84	24.45	6.71
13	44.12	24.78	68.90	22.45	8.65
15	46.08	24.79	70.87	20.23	8.90
18	47.03	24.81	71.84	21.33	6.83
20	45.28	24.81	70.09	21.33	8.58
23	48.21	24.63	72.84	14.98	12.18
25	46.26	26.66	72.92	13.30	13.78

Table 3. Effect of temperature on physicochemical characteristics of bio-oil organic phase*

Temperature (°C)	Density (kg/m^3)	Viscosity (cP)	pH	Water content (%)
400	1,089	14.6	2.6	4.7
450	1,130	18.8	2.6	4.6
500	1,150	25.6	2.9	2.4
550	1,130	23.4	2.6	2.5
600	1,126	21.3	2.8	2.4
650	1,123	18.5	2.9	2.5

*Bio-oil characterization at 25 °C.

This implies that fluidization with helical screw has resulted in high heat and mass transfer rate therefore reaction rates was not affected by the slow feed rates. These findings are comparable with previous studies performed with different feed rates [35]. However, by introducing more PS biomass feed rate above 13 g/min, a noticeable increase in bio-oil, gas yields and decrease in by-product biochar yield. However, the formation of more condensable vapors and gas product with high feed rate is due to the decrease in the vapor residence time inside the reactor, thus preventing from secondary cracking reactions which lead to the a higher bio-oil yield [21]. Treedet et al. also reported that low feed rate resulted in low bio-oil yield and vice versa [36].

3. Characterization of Bio-oil

3-1. Effect of Temperature on Physicochemical Properties of Bio-oil

The typical range of bio-oil density is from 1,000 to 1,240 kg/m^3 at 15 to 40 °C [37]. Based on Table 3, it can be seen that as pyrolysis temperature increased from 400-650 °C, the density of bio-oils improved from 1,089-1,150 kg/cm^3, and as the bio-oil density increased, the content of energy also increased. This result agrees with the results obtained by Bardalai et al. The increase in density is related to the increase in pyrolysis temperature and the decrease in residence time, which provides further biomass breakdown and more vapors [37]. Tanvidkar et al. described that, the development of high liquid density product at high temperatures is linked to low residence time [38]. Viscosity, pH and water content are also important properties of bio-oil, which determine the flow quality or fluidity of the liquid. The viscosity of bio-oil varies in a wide range, as it is produced from various biomasses at different temperatures [39]. The viscosity, pH and water content of bio-oil in this work range from 14.6-25.6 cP, 2.6-2.9 and 2.7-4.7 wt%, respectively.

The results depicted a significant decrease in water content from 4.7% to 2.4% as higher pyrolysis temperature promotes further lignin dehydration. Qiang et al. found that the high amount of water content present in the bio-oil led to phase separation between aqueous phase and heavier organic phase, which makes it difficult to be burnt [40]. Furthermore, high water content in the bio-oil can lower the heating value of the liquid, increase the ignition delay and decrease the combustion rate by decreasing adiabatic flame temperature. Therefore, it is essential to control the water or moisture content to be below 10 wt% [6,41].

3-2. Effect of Feed Rate on Physicochemical Properties of Bio-oil

The effect of feed rate on the product distribution and bio-oil

Table 4. Effect of feed rate on physicochemical characteristics of bio-oil at 500 °C

Feed rate (g/min)		Density (kg/m^3)	Viscosity (cP)	pH	Water content (wt%)
Less	3	1,089	15.8	2.7	6.4
	5	1,120	16.6	2.8	5.5
	7	1,120	16.9	3.0	4.3
Medium	10	1,124	17.8	2.7	4.2
	13	1,124	23.3	3.0	4.2
	15	1,124	21.9	3.0	4.1
High	18	1,127	22.9	3.1	4.0
	20	1,170	23.3	3.1	3.9
	25	1,254	23.8	3.6	2.5

characteristics entirely depends on the particle size, feed rate, reactor configuration [21] and condensation system [37]. Based on Table 4, it can be observed that that there is an increase in density, viscosity, pH and decrease in water content of bio-oil, which indirectly improves the quality of bio-oil. In this HSFBR setup, fluidization efficiency, feed rate and residence time were all directly correlated and affected by the auger speed of the feeding system. With the increase in feed rate, fluidization effect was further increased, which led to better reactant mixing and pyrolysis efficiency to produce bio-oil of higher quality and quantity. In a similar vein, PS biomass would also have lower residence time, which minimizes secondary cracking reactions in producing gaseous products. The decrease in water content might be due to decrease in carbonyls, which can be confirmed from GC-MS analysis. This result agrees with the findings of Yiin et al. [42]. The maximum density was observed at high feed rate from 18 g/min to 25 g/min with high density from 1,127-1,254 kg/m^3, viscosity 22.9-23, pH 3.1-3.6 and a decrease in water content from 4.0-2.5 wt%.

3-3. Ultimate Analysis of Bio-oil at Different Temperatures

Table 5 summarizes the results of ultimate analysis at 400, 500 and 650 °C. The results show that the bio-oil HHV was the lowest at 400 °C, and this could be attributed to the low decomposition of biomass [16]. However, above 400 °C, extensive biomass disintegration was noted, which led to higher de-volatilization of polymers and tar formation [43]. The higher value of HHV at 500 °C could be attributed to the biomass decomposition that enhanced the bio-oil quality. Hossain et al. showed that the increasing temperature improved the percentage of carbon content and HHV [44]. Similar effects of HHV by increasing the pyrolysis temperature have been reported elsewhere [4]. Therefore, when the temperature was further increased from 500 °C to 650 °C a slight increase in HHV of bio-oil from (41.83 to 43.13 MJ/kg) was observed. This can be attributed to the increase of carbon and hydrogen content as well as a noticeable decrease of oxygen content, as can be seen in Table 5. Anguruwa et al. reported that, the yield of bio-oil reduced with the increase in temperature, while calorific value increased with the increase in pyrolysis temperature.

3-4. Ultimate Analysis of Bio-oil at Different Feed Rates

Table 6 reviews the results of ultimate analysis of bio-oil at selected low, medium and high feed rates. The relationship between elemental properties and the biomass feed rate shows that HHV, carbon and hydrogen content were increased while nitrogen, sulfur and oxygen content were decreased when feed rate was increased. These improvements can be attributed to improved heat transfer rate from reactor shell to biomass particle interaction that was delivered by helical screw before biomass particles exited from the reactor hot zone. This result is consistent with the findings of Guedes et al. who described that feed rate correlates with HHV [21]. Xiong et al. reported that, the lower feed rate may decrease pyrolytic vapor formation and movement, which leads to secondary cracking reactions, thus changing the elemental composition and physicochemical properties of bio-oil.

3-5. FTIR Analysis of Bio-oil Obtained at Different Temperatures and Feed Rates

Fig. 3(a) shows the FTIR spectra of bio-oil (organic phase) at pyrolysis temperatures of 400, 500 and 650 °C and Fig. 3(b) shows the FTIR spectra of bio-oil (organic phase) at feed rates of 3, 15 and 25 g/min, respectively. The identified functional groups in

Table 5. Elemental analysis of bio-oil (organic phase) at different temperatures.

	Temperature (°C)	Ultimate analysis of bio-oil (Organic phase) (%)					
		C	H	N	S	O*	HHV (MJ/kg)
Low	400	71.60	10.37	14.7	0.03	3.30	38.52
Medium	500	76.80	11.40	8.37	0.03	3.40	41.83
High	650	79.55	11.83	6.16	0.03	2.43	43.13

*=by difference.

Table 6. Elemental analysis of bio-oil (organic phase) at 500 °C with different feed rate

	Feed rate (g/min)	Ultimate analysis of bio-oil (Organic phase) (%)					
		C	H	N	S	O*	HHV (MJ/kg)
Low	3	76.66	10.23	6.43	0.13	6.55	39.12
Medium	15	78.90	10.21	6.58	0.02	4.29	40.24
High	25	81.80	11.40	3.37	0.03	3.40	43.09

*=by difference.

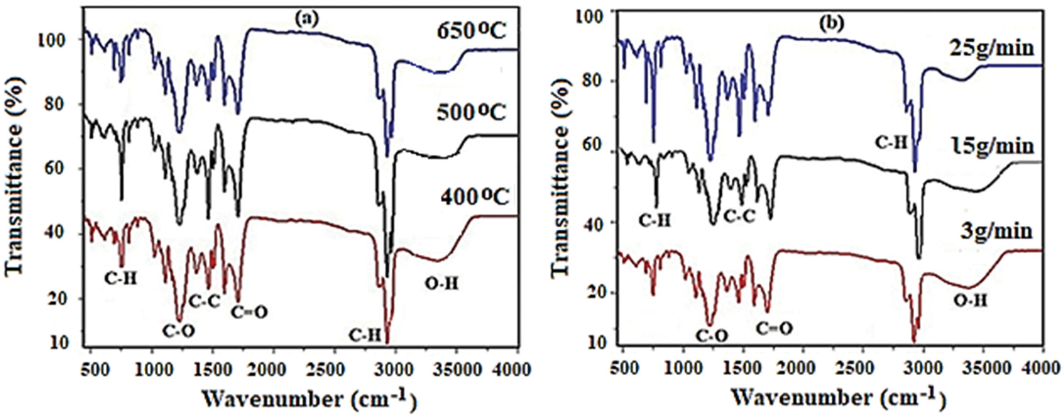

Fig. 3. FTIR spectra of organic phase attained at different (a) temperatures and (b) feed rates.

Table 7. Functional group composition of the bio-oil (organic phase) attained at different temperatures and feed rates

Group	Wavenumber (cm^{-1})	Class of compounds
Alcohols/Phenols	3,000-3,500	O-H Stretch
Aromatics	2,700-3,000	C-H Stretch
Ketones	~1,750	C=O Stretch
Aromatics	~1,500	C-C Stretch
Carboxylic	1,200-1,300	C-O Stretch
Aromatics	~750	C-H medium stretch

bio-oil are summarized in Table 7. The FTIR band assessment indicates the organic phase consists of a number of atomic groups and structures. Band intensities reveal that the most abundant chemical bonds are O-H, C-C, C=O and C-H bonds. The FTIR spectrum of organic phase obtained at 400, 500 and 650 °C indicates O-H stretching vibration between 3,000 cm^{-1} to 3,500 cm^{-1}, which is attributed to phenol group. Generally, phenols are liable for the thermal and chemical instability of bio-oil due to the high oxygen content in the liquid product [32,45-48]. The positive effect in reducing the phenol content is attributed to the higher heat transfer rate and increased temperature from 400 to 500 °C.

Furthermore, a considerable decrease in phenol and increase in aromatics were observed [45], since it can produce value-added chemicals such as aldehydes, acids which improves the energy density and HHV [4]. The results are in agreement with elemental analysis (Table 6). According to Lyu et al., high temperature supports the formation of small aldehydes and acids, accompanied by a reduction of phenols [49]. Besides that, a sharp absorption peak at 500 °C from 1,400-1,500 cm^{-1} with C-H stretching vibration indicates the presence of alkanes, which is high in contrast to the ones obtained at 400 and 650 °C. The 1,750 cm^{-1} band is ascribed to C=O stretching vibration in ketone, indicating the presence of acetyl derivative and aldehyde group [50]. The 1,500 cm^{-1} band relates to C-C stretching, indicating the presence of aromatics. The peak in the range from 1,200-1,300 cm^{-1} with C-O stretching indicates the presence of carboxylic acid. The peak intensity increased when the temperature was increased to 650 °C. Moreover, a medium C-H stretch was noticed, which specifies the existence of aromatics at low frequency region of 750 cm^{-1}.

The O-H stretching vibration between 3,000 cm^{-1} to 3,500 cm^{-1} of phenol group showed a substantial reduction when feed rate was increased from 3 g/min to 25 g/min. This decrease in phenol group was mainly attributed to the nascent char which cracked the oxygenated compound. Hu et al. described that, the nascent char inside the reactor can serve as the catalyst which initiates the secondary cracking of phenol containing vapors, resulting in secondary formation of the bottom organics [51]. Furthermore, C-H, C-C, C-O and C=O peaks at 750 cm^{-1}, 1,500 cm^{-1}, 1,200-1,300 cm^{-1}, 1,750 cm^{-1} bands were shown to increase in peak intensity with the increase in feed rate, indicating higher formation of alkanes, aromatics, ketones and carboxylic acids at higher feeding rate. This improvement in aromatics is due to the extra decomposition of lignin caused by helical screw rotation, which increased the particle-particle and particle-reactor shell interaction during the pyrolysis.

3-6. GC-MS Analysis of Bio-oil at Different Temperatures

The results of GC/MS analysis of bio-oil obtained at 400, 500 and 650 °C are shown in Table 8. Mostly aromatics, alkyls, alcohols, phenols were detected in the samples. The result of this analysis indicates the highest value of possible compounds in alkyls were heptane, methylcyclohexane, ethyl cyclopentane, norbornane and cis-1,2-dimethylcyclopentane respectively. However, at 400 °C a high number of oxygenates, such as cyclohexanol, phenol, 2-methylphenol, 2-methoxyphenol, creosol, 4-ethyl-2-methoxyphenol and 2-,6-dimethoxyphenol, were produced. The oxygenate content was reduced with the increase in pyrolysis temperature. From the results it evidently appears that 500 °C is the optimal temperature to obtain good product quality [10]. Between these chemical constituents, alkenes, aromatics and alkyls are valuable for high-quality bio-oils because of high carbon and hydrogen content that brings a positive effect in HHV enhancement [52]. The existence of these groups signifies the suitability of the oil to be considered for value-added chemicals (e.g., alkyls, aromatic, and alkenes) in bio-oils. In addition, it is necessary to exclude the oxygenates from bio-oil via catalytic upgrading processes such as hydrodeoxygenation, decarboxylation and decarbonylation to improve its energy content [46, 53-55].

3-7. GC-MS Analysis of Bio-oil at Different Feed Rates

Table 9 shows the composition of bio-oil from PS pyrolysis at

Table 8. GC/MS analysis of bio-oil (Organic phase) produced at pyrolysis temperatures of 400, 500 and 650 °C

Identified compounds and groups	Chemical formula	Relative content (%) Temperature (°C)			Identified compounds and groups	Chemical formula	Relative content (%) Temperature (°C)		
		400	500	650			400	500	650
Aromatics					Ketones				
Toluene	C_7H_8	13.12	18.59	16.64	Cyclohexanone	$C_6H_{10}O$	2.51	1.32	1.52
Benzene, 1,2,4-trimethoxy-	$C_9H_{12}O_3$	2.32	1.21	2.01	7-Oxabicyclo[2.2.1]heptane	$C_6H_{10}O$	2.57	1.03	1.24
Benzene, 1,2,3-trimethoxy-5-methyl-	$C_{10}H_{14}O_3$	2.53	1.54	1.12	7-Oxabicyclo[4.1.0]heptane	$C_6H_{10}O$	3.52	0.37	1.84
Total		17.97	21.34	19.77	2,5-Dimethylfuran	C_6H_8O	3.16	1.34	4.10
Alkanes					Total		11.76	4.06	10.38
Heptane	C_7H_{16}	3.45	7.61	6.37	Alkenes				
Cyclohexane, methyl-	C_7H_{14}	4.12	8.51	7.79	Cyclohexene	C_6H_{10}	4.07	5.62	6.21
Cyclopentane, ethyl-	C_7H_{14}	3.23	6.53	7.53	2-Hexene, 4-methyl-, (E)-	C_7H_{14}	2.53	7.77	6.12
Norbornane	C_7H_{12}	1.56	3.62	1.23	Total		6.60	13.39	12.33
Cyclopentane, 1,2-dimethyl-, cis-	C_7H_{14}	3.85	4.38	4.61	Aldehydes				
Total		16.21	30.65	27.53	5-Hexenal	$C_6H_{10}O$	4.1	3.15	2.70
Alcohols and Phenols					Hexanal	$C_6H_{10}O$	1.1	0.25	0.57
Cyclohexanol	$C_6H_{12}O$	1.68	1.67	1.12	Furfural	$C_5H_4O_2$	2.3	1.3	1.52
Phenol	C_6H_6O	17.30	15.35	13.44	Total		7.5	4.7	4.79
Phenol, 2-methyl-	C_7H_8O	1.31	2.12	1.12	Esters				
Phenol, 2-methoxy-	$C_7H_8O_2$	1.96	-	1.34	Dodecanoic acid, methyl ester	$C_{13}H_{26}O_2$	4.31	1.87	1.34
Creosol	$C_8H_{10}O_2$	1.10	-	1.11	2,4-Hexadienedioic acid, 3,4-diethyl-, dimethyl ester, (E,Z)-	$C_{12}H_{18}O_4$	3.73	2.73	1.87
Phenol, 4-ethyl-2-methoxy-	$C_9H_{12}O_2$	1.21	0.11	0.87	Tetradecanoic acid, methyl ester	$C_{15}H_{30}O_2$	5.46	2.01	2.99
Phenol, 2,6-dimethoxy-	$C_8H_{10}O_3$	1.90	-	-	Total		13.50	6.61	6.20
Total		26.46	19.25	19.00	Grand Total		100	100	100

different feed rates as analyzed via GC/MS. A total of seven groups, including 29 kinds of major compounds, were identified. When feed rate was increased, the yield of deoxygenated products (aromatics, alkanes, alkenes) increased, while the yield of oxygenated products (alcohols, phenols, ketones, esters, aldehydes) decreased. In addition, the yield ratio of deoxygenated non-aromatics (alkanes and alkenes) to deoxygenated aromatics was 2.04, 3.52 and 3.70 at the respective feeding rates of 3, 15 and 25 g/min. The changes in liquid product composition at higher feed rates are attributed to the enhanced heat transfer rate by particle-particle and particle-reactor hot shell interaction, which triggered the greater extent of ring opening, dehydration and cracking of heavy oxygenated aromatics molecule [56]. The increase in selectivity for deoxygenated non-aromatics at higher feed rate is a favorable trend in producing liquid fuel of better quality, as deoxygenated non-aromatics have higher HHV than their aromatic counterparts [48].

4. Characterization of Biochar

4-1. Effect of Temperature on Physicochemical Properties of Biochar

Table 10 shows that the by-product biochar obtained at 400 °C has a carbon content around 60.12% and it has highest volatile matter of 72.85%. As pyrolysis temperature increased to 500 °C, carbon, oxygen and volatile matter contents were reduced. This is because higher pyrolysis temperature enables higher volatilization of carbon and volatile matters in PS to form bio-oil instead of bio-char. Pyrolysis result at 500 °C shows that by-product biochar produced has highest carbon content with significantly higher HHV 30 MJ/kg, since it can add the HHV [57]. These results are consistent with the results of Rafiq et al. for carbon stability of the by-product biochar attained at different temperatures [58]. Furthermore, FTIR analysis also confirmed the presence of more alkene, alkane and aromatics in the by-product biochar produced at 500 °C. Thus, biomass pyrolysis temperature at 500 °C produced maximum bio-oil as main product and by-product biochar that could be a prom-

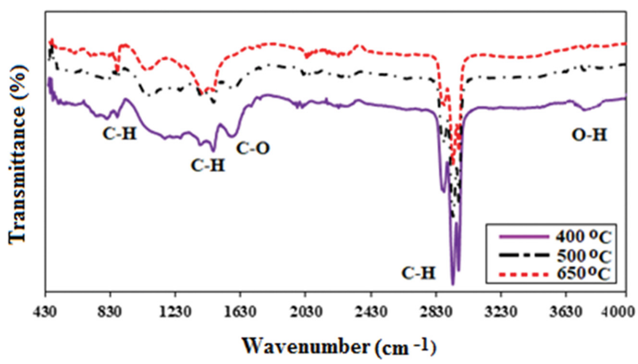

Fig. 4. FTIR spectra of the by-product biochar attained at different temperatures.

Table 9. GC/MS analysis of bio-oil (Organic phase) produced at different feed rates

Identified compounds and groups	Chemical formula	Relative content (%) Feed rate (g/min) 3	15	25	Identified compounds and groups	Chemical formula	Relative content (%) Feed rate (g/min) 3	15	25
Aromatics					Ketones				
Toluene	C_7H_8	5.89	6.30	10.38	Cyclopentenone	C_5H_6O	2.21	1.01	1.67
Benzene, 1,2,4-trimethoxy	$C_9H_{12}O_3$	3.32	4.34	1.21	Cyclohexanone	$C_6H_{10}O$	2.51	1.52	1.32
Benzene, 1,2,3-trimethoxy-5-methyl-	$C_{10}H_{14}O_3$	4.53	3.12	2.52	7-Oxabicyclo[2.2.1]heptane	$C_6H_{10}O$	2.57	1.24	1.03
Total		13.74	13.76	14.11	7-Oxabicyclo[4.1.0]heptane	$C_6H_{10}O$	3.52	2.84	1.37
Alkanes					2,5-Dimethylfuran	C_6H_8O	3.16	3.10	2.34
Cyclohexane	C_6H_{12}	5.23	6.01	8.21	Total		13.97	9.71	7.73
Heptane	C_7H_{16}	3.45	6.37	7.61	Alkenes				
Cyclohexane, methyl-	C_7H_{14}	4.12	7.79	8.51	Cyclohexene	C_6H_{10}	4.07	5.21	5.62
Cyclopentane, ethyl-	C_7H_{14}	5.23	7.53	6.53	2-Hexene, 4-methyl-, (E)-	C_7H_{14}	2.53	6.12	7.77
Norbornane	C_7H_{12}	3.56	2.23	3.71	Total		6.6	11.33	13.39
Cyclopentane, 1,2-dimethyl-, cis-	C_7H_{14}	3.85	4.61	4.38	Aldehydes				
Total		25.44	34.54	38.95	5-Hexenal	$C_6H_{10}O$	4.10	2.15	2.70
Alcohols and Phenols					Hexanal	$C_6H_{10}O$	0.57	1.25	1.27
Cyclohexanol	$C_6H_{12}O$	1.68	1.12	1.67	Furfural	$C_5H_4O_2$	3.40	1.30	1.52
Phenol	C_6H_6O	15.30	13.44	10.43	Total		8.07	4.70	5.49
Phenol, 2-methyl-	C_7H_8O	1.31	1.99	2.12	Esters				
Phenol, 2-methoxy-	$C_7H_8O_2$	1.96	1.34	3.12	Dodecanoic acid, methyl ester	$C_{13}H_{26}O_2$	4.31	2.14	1.34
Creosol	$C_8H_{10}O_2$	2.7	3.11	3.44	2,4-Hexadienedioic acid, 3,4-diethyl-, dimethyl ester, (E,Z)-	$C_{12}H_{18}O_4$	3.73	2.73	1.87
Phenol, 4-ethyl-2-methoxy-	$C_9H_{12}O_2$	1.21	0.87	3.86	Tetradecanoic, methyl ester	$C_{15}H_{30}O_2$	4.68	2.01	2.99
Phenol, 2,6-dimethoxy-	$C_{11}H_{14}O_3$	1.90	3.54	2.88	Total		12.72	6.88	6.20
Total		26.06	30.41	27.52	Grand Total		100	100	100

Table 10. Ultimate and proximate analysis of by-product biochar at different pyrolysis temperatures

	Temperature (°C/min) 400	500	650
Ultimate analysis (wt%)			
C	60.98	54.64	57.45
H	2.73	8.57	7.21
N	0.43	1.97	1.28
S	0.03	0.02	0.67
O*	35.83	34.8	33.39
Proximate analysis (wt%)			
Moisture content	4.90	7.94	8.20
Volatile matter (by difference)	72.85	70.21	69.59
Fixed carbon	18.5	20.84	20.46
Ash	3.75	1.01	1.13
HHV (MJ/kg)	23.14	30.00	23.81
LHV (MJ/kg)	22.54	28.13	22.23

*=by difference

Table 11. Functional groups of by-product biochar

Group	Wavenumber (cm^{-1})	Class of compounds
Alcohols/Phenol	3,640-3,800	O-H Stretch
Alkanes	2,924-2,969	C-H Stretch
Carboxylic	1,600-1,630	C-O Stretch
Alkynes	~1,500	C-H Stretch
Aromatics	~840	C-H Stretch

ising approach to liquid and solid fuel production.

Fig. 4 displays the FTIR spectra of by-product biochar derived from PS pyrolysis at 400, 500 and 650 °C along with their functional group identifications as shown in Table 11. The FTIR spectrum of by-product biochar at 400 °C showed significant O-H stretch intensity in the range of (3,640-3,800 cm^{-1}), while an increase in temperature caused a significant decrease in phenolics. Hamza et al. also reported a similar trend and attributed it to the greater extent of hemicellulose and cellulose breakdown at higher pyrolysis temperature [59]. At higher pyrolysis temperature, the higher volatilization of PS biomass causes the carbon content to be concentrated in the bio-oil instead of bio-char, causing a decrease in the carbon content of biochar. Thus, the selection of pyrolysis temperature must be based on the desired pyrolytic product phase.

Based on Fig. 5, Table 12 and 13, the primary weight loss at temperature range of 25-200 °C is attributed to moisture and volatiles

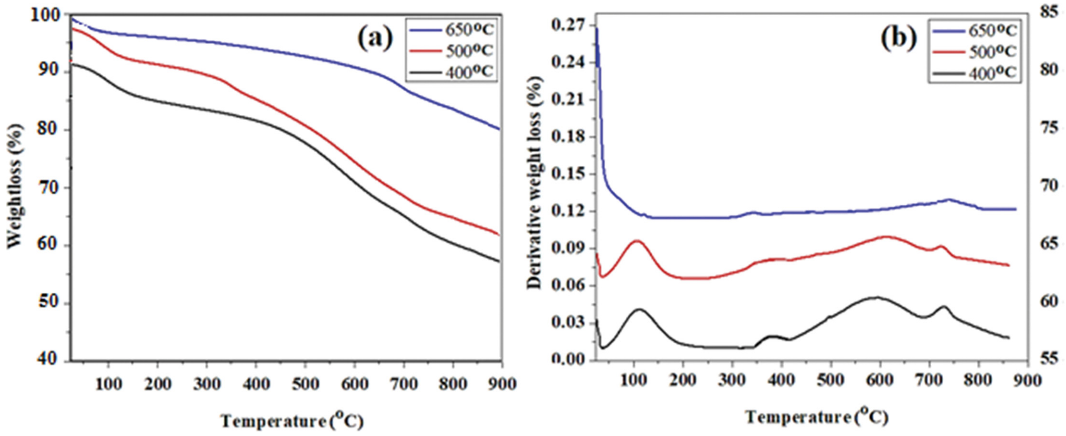

Fig. 5. (a) TGA analysis and (b) DTG analysis of by-product biochar obtained at 400, 500 and 650 °C.

Table 12. Weight loss of by-product biochar samples obtained at different temperatures

Pyrolysis temperature (°C)	Weight loss (%)			Total weight loss (%)	Residue (%)
	1 (25-200 °C)	2 (200-700 °C)	3 (700-900 °C)		
400	12	25	10	36	64
500	7	10	3	20	80
650	5	2	2	9	91

Table 13. DTG analysis of by-product biochar obtained at different temperatures

Peak No.	Temperature (°C)			Temprature range (°C)	Content
	400	500	650		
	Derivative weight loss (%)				
1	0.05	0.04	-	25-200	Moisture and volatile
2	0.02	0.02	0.003	200-430	Hemicellulose, cellulose and lignin
3	0.06	0.03	0.005	430-700	Hemicellulose, cellulose and lignin
4	0.05	0.01	-	700-750	Lignin

evaporation within biochar. The second major weight loss in temperature range of 200-700 °C corresponds to hemicellulose and lignin decomposition. The third major weight loss at temperature range of 700-900 °C corresponds to the further decomposition of lignin in biochar. The second major weight loss shows the decomposition of hemicellulose, cellulose and lignin over a broad temperature range with smaller distinct DTG peaks, which can be accounted for the respective decomposition of such components within this temperature range. Earlier studies also revealed the major weight loss of hemicellulose takes place from 400-430 °C [60,61]. Biochar sample obtained at 650 °C has the least weight loss since most of the biomass components have been converted to pyrolytic products within the bio-oil.

4-2. Effect of Feed Rate on Physicochemical Properties of Biochar

Table 14 shows that the carbon, hydrogen content and heating values decreased when feed rate was increased. Higher feeding rate was indicated in the previous sections to improve volatilization of biomass components to form bio-oil, which in turn reduces the available components within the biochar. A similar trend was also shown in FTIR spectra (Fig. 6), where hydrocarbon functional

Table 14. Ultimate and proximate analysis of by-product biochar with different feed rates

Characteristics	Feed rate (g/min)		
	5	15	25
Ultimate analysis (wt%)			
C	60.98	57.45	54.64
H	8.73	8.21	6.57
N	0.42	1.28	1.97
S	0.03	0.67	0.02
O*	29.84	32.39	36.8
Proximate analysis (wt%)			
Moisture content	10.20	10.94	11.90
Volatile matter*	67.45	67.21	65.85
Fixed carbon	20.46	19.51	19.50
Ash	1.89	2.34	2.75
HHV (MJ/kg)	27.83	25.43	21.32
LHV (MJ/kg)	25.92	23.64	19.88

*=by difference

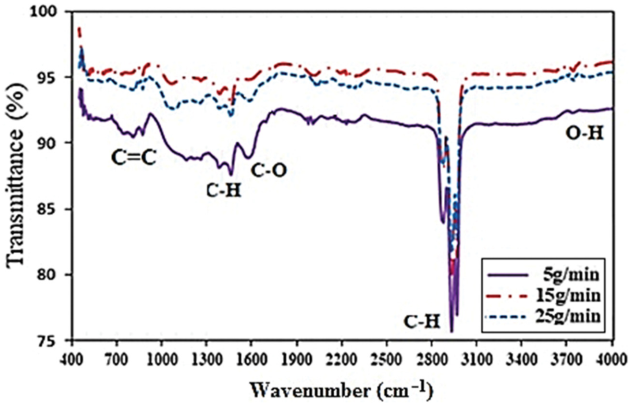

Fig. 6. FTIR spectra of the by-product biochar attained at different feed rates.

groups within biochar generally decreased in amount as feed rate increased. This is in corroboration with GC-MS analysis of bio-oil sample (Table 9) where most of the hydrocarbons were produced within bio-oil phase. The increase in oxygen content of biochar at higher feed rate could also indicate the retention of oxygen during its catalytic cracking of oxygenates in bio-oil yield [62].

Based on Fig. 7, Table 15 and 16, the primary weight loss in the temperature range of 20-150 °C is attributed to moisture and volatiles evaporation within biochar. The second and third major weight losses intemperature ranges of 200-390 °C and 390-550 °C corresponds to the decomposition of hemicellulose, cellulose and lignin. The fourth major weight loss at temperature range of 550-800 °C corresponds to the further decomposition of lignin in biochar. Similar weight loss trends were also reported in Section 3.4.1. When feed rate is increased, the greater extent of biomass causes most of the biomass components to be converted to pyrolytic products within the bio-oil instead of in biochar.

CONCLUSION

We performed a parametric study on the effects of pyrolysis temperature and biomass feeding rate on the production of PS-derived bio-oil by helical screw fluidized bed reactor. The results show that

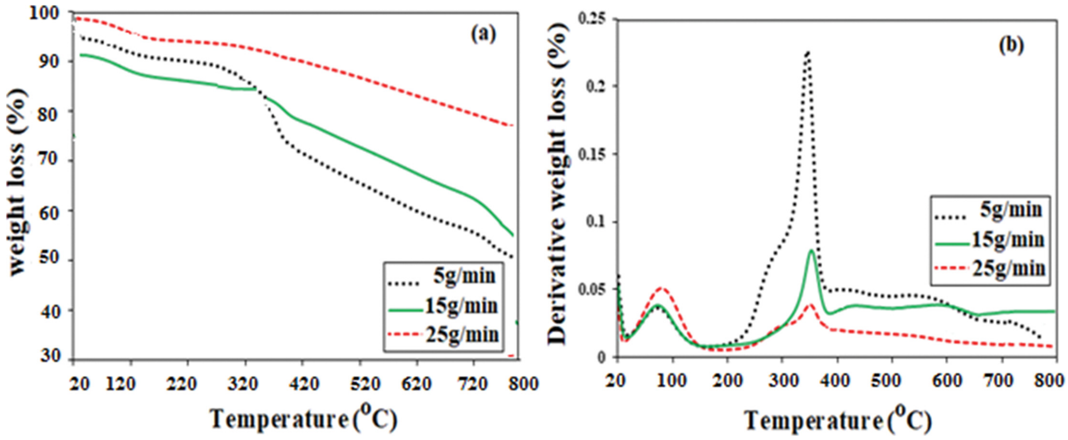

Fig. 7. (a) TGA analysis and (b) DTG analysis of by-product biochar attained with 5 g/min, 15 g/min and 25 g/min.

Table 15. TGA analysis of by-product biochar samples obtained with different feed rates

Feed rate (g/min)	Weight loss (%)				Total weight loss (%)	Residue (%)
	1 (20-150 °C)	2 (200-390 °C)	3 (390-550 °C)	4 (550-800 °C)		
5	3	10	10	2	25	75
15	2	4	3	-	9	91
25	1	1	2	-	4	96

Table 16. DTG analysis of by-product biochar obtained with different feed rates

Peak No.	Feed rate (g/min)			Temprature range (°C)	Content
	5	15	25		
	Derivative weight loss (%)				
1	0.05	0.04	0.05	20-150	Moisture and volatile
2	0.24	0.07	0.03	200-390	Hemicellulose, cellulose and lignin
3	0.05	0.03	0.01	390-550	Hemicellulose, cellulose and lignin
4	0.03	0.01	-	550-800	Lignin

the temperature and the feed rate have significant effects on the bio-oil yield and physicochemical properties of pyrolytic products. When pyrolysis temperature or feed rate was increased, the yields of bio-oil and gas were increased while biochar yield was decreased. The increase in these parameters enabled better heat transfer rate and reactant mixing to promote biomass volatilization. FTIR and GC/MS analyses indicated the presence of aromatics, alkanes, alkenes, alcohols, phenols, ketones, aldehydes, acids and esters within the bio-oil and the biochar. The enhanced biomass volatilization at higher feed rate and pyrolysis temperature also resulted in greater extent in oxygenate cracking to produce bio-oil of higher heating values, carbon, hydrogen contents and lower oxygen content. With the production of bio-oil at higher quantity and quality at these settings, the biochar was noted to decrease in its yield and quality as most of the pyrolytic products were volatilized and concentrated in the liquid product. The presence of oxygenate residue within bio-oil also indicates the necessity of subsequent oxygen removal process such as hydrodeoxygenation to further reduce the oxygen content and increase the heating value of bio oil so as to be comparative with the properties of conventional liquid fuel.

ACKNOWLEDGEMENTS

The authors thank GSP-MOHE, University of Malaya for funding this study through the project number MO008-2015. This work is also supported by Xiamen University Malaysia Research Fund (Grant No: XMUMRF/2021-C7/IENG/0032).

REFERENCES

1. A. Ayala-Cortés, D. R. Lobato-Peralta, C. E. Arreola-Ramos, D. C. Martínez-Casillas, D. E. Pacheco-Catalán, A. K. Cuentas-Gallegos, C. A. Arancibia-Bulnes and H. I. Villafán-Vidales, *J. Anal. Appl. Pyrolysis*, **140**, 290 (2019).
2. T. Miranda, I. Montero, F. J. Sepúlveda, J. I. Arranz, C. V. Rojas and S. Nogales, *Mater. (Basel, Switzerland)*, **8**, 1413 (2015).
3. F. Abnisa, A. Arami-Niya, W. W. Daud, J. Sahu and I. Noor, *Energy Convers. Manage.*, **76**, 1073 (2013).
4. K. M. Qureshi, F. Abnisa and W. M. A. Wan Daud, *J. Anal. Appl. Pyrolysis*, **142**, 104605 (2019).
5. J. Akhtar and N. S. Amin, *Renew. Sustain. Energy Rev.*, **16**, 5101 (2012).
6. K. M. Qureshi, A. N. Kay Lup, S. Khan, F. Abnisa and W. M. A. W. Daud, *J. Anal. Appl. Pyrolysis*, **131**, 52 (2018).
7. Z. Xiong, S. S. A. Syed-Hassan, X. Hu, J. Guo, Y. Chen, Q. Liu, Y. Wang, S. Su, S. Hu and J. Xiang, *Fuel*, **233**, 461 (2018).
8. M. N. Uddin, K. Techato, J. Taweekun, M. M. Rahman, M. G. Rasul, T. M. I. Mahlia and S. M. Ashrafur, *Energies*, **11**, 3115 (2018).
9. M. I. Jahirul, M. G. Rasul, A. A. Chowdhury and N. Ashwath, *Energies*, **5**, 4952 (2012).
10. K. M. Qureshi, A. N. Kay Lup, S. Khan, F. Abnisa and W. M. A. Wan Daud, *Cleaner Eng. Technol.*, **4**, 100174 (2021).
11. J. I. Montoya, F. Chejne-Janna and M. Garcia-Pérez, *DYNA*, **82**, 239 (2015).
12. C. Quan and N. Gao, *BioMed Res. Int.*, **2016**, 6197867 (2016).
13. Y. Wang, L. Qiu, M. Zhu, G. Sun, T. Zhang and K. Kang, *Sci. Rep.*, **9**, 5535 (2019).
14. C. Z. Zaman, K. Pal, W. A. Yehye, S. Sagadevan, S. T. Shah, G. A. Adebisi, E. Marliana, R. F. Rafique and R. B. Johan, in *Pyrolysis*, M. Samer Ed., IntechOpen Limited, London (2017).
15. A. V. Bridgwater, *Biomass Bioenergy*, **38**, 68 (2012).
16. T. Kan, V. Strezov and T. J. Evans, *Renew. Sustain. Energy Rev.*, **57**, 1126 (2016).
17. N. Bhattacharjee and A. B. Biswas, *J. Energy Inst.*, **91**, 605 (2018).
18. S. Mutsengerere, C. H. Chihobo, D. Musademba and I. Nhapi, *Renew. Sustain. Energy Rev.*, **104**, 328 (2019).
19. A. Heidari, R. Stahl, H. Younesi, A. Rashidi, N. Troeger and A. A. Ghoreyshi, *J. Ind. Eng. Chem.*, **20**, 2594 (2014).
20. R. Zhou, H. Lei and J. L. Julson, *Int. J. Agric. Biol. Eng.*, **6**, 53 (2013).
21. R. E. Guedes, A. S. Luna and A. R. Torres, *J. Anal. Appl. Pyrolysis*, **129**, 134 (2018).
22. Q. Xiong, S. Aramideh and S.-C. Kong, *Energy Fuels*, **27**, 5948 (2013).
23. K. M. Qureshi, F. Abnisa and W. M. A. Wan Daud, *J. Anal. Appl. Pyrolysis*, **142**, 104605 (2019).
24. F. Abnisa, W. M. A. W. Daud, W. N. W. Husin and J. N. Sahu, *Biomass Bioenergy*, **35**, 1863 (2011).
25. M. S. A. Moraes, D. Tomasini, J. M. da Silva, M. E. Machado, L. C. Krause, C. A. Zini, R. A. Jacques and E. B. Caramao, in *Frontiers in bioenergy and biofuels*, E. Jacob-Lopes and L. Q. Zepka Eds., IntechOpen Limited, London (2017).
26. Y. Lu, G.-S. Li, Y.-C. Lu, X. Fan and X.-Y. Wei, *Int. J. Anal. Chem.*, **2017**, 9298523 (2017).
27. J. I. Montoya, F. Chejne-Janna and M. Garcia-Perez, *DYNA*, **82**, 239 (2015).
28. E. Ranzi, A Cuoci, T Faravelli, A. Frassoldati, G. Migliavacca, S. Pierucci and S. Sommariva, *Energy Fuels*, **22**, 4292 (2008).
29. C. Branca and C. Di Blasi, *Ind. Eng. Chem. Res.*, **45**, 5891 (2006).
30. A. V. Bridgwater, *Biomass Bioenergy*, **38**, 68 (2012).
31. R. V. Powar and S. Gangil, *Int. J. Renew. Energy Res.*, **3**, 519 (2013).
32. S. W. Kim, B. S. Koo, J. W. Ryu, J. S. Lee, C. J. Kim, D. H. Lee, G. R. Kim and S. Choi, *Fuel Process. Technol.*, **108**, 118 (2013).
33. P. T. Williams and E. A. Williams, *J. Anal. Appl. Pyrolysis*, **51**, 107 (1999).
34. S. Zhou, M. Garcia-Perez, B. Pecha, A. G. McDonald, S. R. A. Kersten and R. J. M. Westerhof, *Energy Fuels*, **27**, 1428 (2013).
35. S. Jalalifar, R. Abbassi, V. Garaniya, K. Hawboldt and M. Ghiji, *Fuel*, **234**, 616 (2018).
36. W. Treedet and R. Suntivarakorn, *Fuel Process. Technol.*, **179**, 17 (2018).
37. M. Bardalai and D. K. Mahanta, *Int. J. Renew. Energy Res.*, **5**, 277 (2015).
38. P. S. Tanvidkar, *Catalytic up-gradation of bio-oil by pyrolysis of biomass*, Master, Chemical Engineering, National Institute of Technology Rourkela Odisha, India (2015).
39. M. Bertero, H. A. Gorostegui, C. J. Orrabalis, C. A. Guzmán, E. L. Calandri and U. Sedran, *Fuel*, **116**, 409 (2014).
40. Q. Lu, W.-Z. Li and X.-F. Zhu, *Energy Convers. Manage.*, **50**, 1376 (2009).
41. M. Ringer, V. Putsche and J. Scahill, *Large-scale pyrolysis oil production: A technology assessment and economic analysis*, National Renewable Energy Lab. (NREL), Golden, CO (United States) (2006).

42. C. L. Yiin, S. Yusup, P. Udomsap, B. Yoosuk and S. Sukkasi, *Computer Aided Chem. Eng.*, **33**, 223 (2014).
43. K. Kundu, A. Chatterjee, T. Bhattacharyya, M. Roy and A. Kaur, in *Prospects of alternative transportation fuels*, A. P. Singh, R. A. Agarwal, A. K. Agarwal, A. Dhar and M. K. Shukla Eds., Springer, Singapore (2018).
44. F. M. Hossain, J. Kosinkova, R. J. Brown, Z. Ristovski, B. Hankamer, E. Stephens and T. J. Rainey, *Energies*, **10**, 467 (2017).
45. A. N. Kay Lup, F. Abnisa, W. M. A. W. Daud and M. K. Aroua, *Asia-Pacific J. Chem. Eng.*, **14**, e2293 (2019).
46. S. Khan, A. N. Kay Lup, K. M. Qureshi, F. Abnisa, W. M. A. Wan Daud and M. F. A. Patah, *J. Anal. Appl. Pyrolysis*, **140**, 1 (2019).
47. A. N. Kay Lup, F. Abnisa, W. M. A. Wan Daud and M. K. Aroua, *J. Ind. Eng. Chem.*, **56**, 1 (2017).
48. A. N. Kay Lup, F. Abnisa, W. M. A. W. Daud and M. K. Aroua, *Appl. Catal. A: Gen.*, **541**, 87 (2017).
49. G. Lyu, S. Wu and H. Zhang, *Front. Energy Res.*, **3**, 28 (2015).
50. P. Fu, S. Hu, J. Xiang, P. Li, D. Huang, L. Jiang, A. Zhang and J. Zhang, *J. Anal. Appl. Pyrolysis*, **88**, 117 (2010).
51. C. Hu, H. Zhang and R. Xiao, *Energy Convers. Manage.*, **177**, 765 (2018).
52. S. H. Chang, *Biomass Bioenergy*, **119**, 263 (2018).
53. J. O. Ogunkanmi, D. M. Kulla, N. O. Omisanya, M. Sumaila, D. O. Obada and D. Dodoo-Arhin, *Case Studies Therm. Eng.*, **12**, 711 (2018).
54. A. N. Kay Lup, F. Abnisa, W. M. A. Wan Daud and M. K. Aroua, *Acidity, oxophilicity and hydrogen sticking probability of supported metal catalysts for hydrodeoxygenation process*, presented at the 3rd ICChESA 2017: Materials Science and Engineering (2018).
55. A. N. Kay Lup, F. Abnisa, W. M. A. W. Daud and M. K. Aroua, *Chin. J. Chem. Eng.*, **27**, 349 (2019).
56. L. Fan, Y. Zhang, S. Liu, N. Zhou, P. Chen, Y. Cheng, M. Addy, Q. Lu, M. M. Omar, Y. Liu, Y. Wang, L. Dai, E. Anderson, P. Peng, H. Lei and R. Ruan, *Bioresour. Technol.*, **241**, 1118 (2017).
57. T. Miranda, I. Montero, F. J. Sepúlveda, J. I. Arranz, C. V. Rojas and S. Nogales, *Materials*, **8**, 1413 (2015).
58. M. K. Rafiq, R. T. Bachmann, M. T. Rafiq, Z. Shang, S. Joseph and R. Long, *PloS One*, **11**, e0156894 (2016).
59. U. D. Hamza, N. S. Nasri, N. S. Amin, J. Mohammed and H. M. Zain, *Desalin. Water Treat.*, **57**, 7999 (2016).
60. H. Yang, R. Yan, H. Chen, D. H. Lee and C. Zheng, *Fuel*, **86**, 1781 (2007).
61. Y. Lu, Y.-C. Lu, H.-Q. Hu, F.-J. Xie, X.-Y. Wei and X. Fan, *J. Spectroscopy*, **2017**, 1 (2017).
62. S.-J. Kim, S.-H. Jung and J.-S. Kim, *Bioresour. Technol.*, **101**, 9294 (2010).